Journal of Applied Physics

Enhanced ferroelectricity, piezoelectricity, and ferromagnetism in Nd-modified $BiFeO_3$-$BaTiO_3$ lead-free ceramics

Cite as: J. Appl. Phys. **116**, 184101 (2014); https://doi.org/10.1063/1.4901198
Submitted: 07 August 2014 . Accepted: 24 October 2014 . Published Online: 10 November 2014

Qiaoji Zheng, Lingling Luo, Kwok Ho Lam, Na Jiang, Yongquan Guo, and Dunmin Lin

Enhanced ferroelectricity, piezoelectricity, and ferromagnetism in Nd-modified $BiFeO_3$-$BaTiO_3$ lead-free ceramics

Qiaoji Zheng,[1] Lingling Luo,[1] Kwok Ho Lam,[2] Na Jiang,[1] Yongquan Guo,[1] and Dunmin Lin[1,a)]

[1]*College of Chemistry and Materials Science, Sichuan Normal University, Chengdu 610066, China*
[2]*Department of Electrical Engineering, The Hong Kong Polytechnic University, Hunghom, Kowloon, Hong Kong*

(Received 7 August 2014; accepted 24 October 2014; published online 10 November 2014)

Lead-free multiferroic ceramics of $0.75Bi_{1-x}Nd_xFeO_3 - 0.25BaTiO_3 + 1$ mol. % MnO_2 were prepared by a conventional ceramic technique and their structure, piezoelectricity, and multiferroicity were studied. The ceramics sintered at 890–990 °C possess a pure perovskite structure. A morphotropic phase boundary of rhombohedral and monoclinic phases is formed at $x = 0.05$. A small amount of Nd improves the ferroelectric and piezoelectric properties of the ceramics. The ferroelectric-paraelectric phase transition becomes gradually diffusive with x increasing. After the addition of Nd, the ferromagnetism of the ceramics is greatly enhanced by ~320%. The increase in sintering temperature improves significantly the ferroelectric, piezoelectric, and ferromagnetic properties of the ceramics. The ceramics with $x = 0.05$ sintered at 950–990 °C possess improved ferroelectricity, piezoelectricity, magnetism and insulation with P_r of 16.5–17.5 $\mu C/cm^2$, d_{33} of 113–121 pC/N, M_r of 0.127–0.138 emu/g, R of $\sim 5 \times 10^9$ Ω·cm and high T_C of 473–482 °C, indicating that the ceramic is a promising candidate for room-temperature multiferroic and high-temperature piezoelectric materials. © *2014 AIP Publishing LLC*.
[http://dx.doi.org/10.1063/1.4901198]

I. INTRODUCTION

In recent years, lead-free piezoelectric and ferroelectric ceramics have received considerable attention because of environmental protection. $BaTiO_3$-,[1] $Bi_{0.5}Na_{0.5}TiO_3$-,[2] and $K_{0.5}Na_{0.5}TiO_3$-[3] based ceramics are considered as promising candidates for lead-free materials due to their good piezoelectricity. However, these materials usually exhibit the poor temperature stability of piezoelectric properties because of their room temperature coexistence of tetragonal and orthorhombic phases or low depolarization/Curie temperature.[1–3] Therefore, there is an increasing interest to develop lead-free materials with high Curie temperature.

Because of the simultaneous existence of ferromagnetism and ferroelectricity, perovskite $BiFeO_3$ has been extensively investigated and exhibits potential multifunctional applications with various advanced devices.[4–8] $BiFeO_3$ possesses the very high Curie temperature T_C of 830 °C and Néel temperature T_N of 370 °C,[9] suggesting that it may be a promising candidate for lead-free multiferroic and high temperature piezoelectric materials. However, pure $BiFeO_3$ ceramic usually exhibits high electrical leakage because of the reduction of Fe ions from Fe^{3+} to Fe^{2+} during sintering and the formation of oxygen vacancies for charge compensation,[10–13] leading to difficulties in obtaining saturated polarization hysteresis loop and electric poling for evaluating the piezoelectric response of the material. In addition, due to the narrow temperature range of phase stabilization, $BiFeO_3$ ceramic with pure perovskite phase is difficult to synthesize and some impurity phases usually exist in the $BiFeO_3$ ceramic.[9–11] In order to increase the electric resistivity and inhibit the formation of impurity phases of $BiFeO_3$-based materials, a lot of investigations have been carried out; these include the use of various fabrication techniques,[9,13,14] the partial substitutions of analogous ions for Bi^{3+} and Fe^{3+} in the $BiFeO_3$ lattices[15–19] and the formation of solid solutions of $BiFeO_3$ with ABO_3-type perovskites.[20–24] Among $BiFeO_3$-based solid solutions, $BiFeO_3$-$BaTiO_3$ is a classic mutliferroic system that has been frequently investigated.[20,25–29] However, these studies mainly focused on dielectric and magnetic properties and rarely show saturated ferroelectric hysteresis loops and considerable piezoelectric response because of the difficulty in electric poling caused by poor electric insulation of the materials.[25–29] Recently, Leontsev[30] and Zhou[31] *et al.* reported Mn-doped $BiFeO_3$-$BaTiO_3$ with good piezoelectricity. However, there are few reports on $BiFeO_3$-based ceramics with the simultaneous existence of good ferromagnetism, strong ferroelectricity, and large piezoelectricity. It has been noted that the partial substitution of rare earth ions for Bi^{3+} (e.g., La^{3+}, Sm^{3+}, Nd^{3+}, etc.) in $BiFeO_3$ can enhance the ferromagnetism and ferroelectricity of the materials.[17,32–35] Therefore, it can be reasonably expected that Nd^{3+} doping may improve the properties of $BiFeO_3$-$BaTiO_3$. To our knowledge, there is no report on Nd-modified $BiFeO_3$-$BaTiO_3$ ceramic and its structure, piezoelectric and multiferroic properties. In the present work, $0.75Bi_{1-x}Nd_xFeO_3 - 0.25BaTiO_3 + 1$ mol. %MnO_2 ceramics were prepared by a conventional sintering technique in air and the microstructural, electrical, and magnetic properties of the ceramics were studied. On the basis of the reported work,[30,31]

a)Author to whom correspondence should be addressed. E-mail: ddmd222@sicnu.edu.cn. Tel.: +86 28 84760802. Fax: +86 28 84767868

1 mol. % MnO_2 was added to increase the resistivity of the ceramics.

II. EXPERIMENTAL

Lead-free multiferroic ceramics of $0.75Bi_{1-x}Nd_xFeO_3 - 0.25BaTiO_3 + 1$ mol. % MnO_2 (BFO-BT-Nd-x) were prepared by a conventional ceramic fabrication technique using metal oxides and carbonate powders as raw materials: Bi_2O_3 (99.9%), Nd_2O_3 (99.9%), Fe_2O_3 (99%), $BaCO_3$ (99%), TiO_2 (99.9%), and MnO_2 (99%). The powders were weighed in the stoichiometric ratio of $0.75Bi_{1-x}Nd_xFeO_3 - 0.25BaTiO_3$, mixed thoroughly in ethanol using zirconia balls for 12 h, then dried and calcined at 800 °C for 4 h. After the calcination, MnO_2 powder was added. The mixture was ball-milled again for 12 h, mixed thoroughly with a poly(vinyl alcohol) binder solution, and then pressed into disk samples. After removal of the binder at 650–700 °C, the samples were sintered at 890–990 °C for 2 h in air. Silver electrodes were fired on both surfaces of the sintered ceramics at 650 °C for 15 min. The samples were poled at 120 °C for 20 min and then cooled to room temperature in a silicone oil bath under a dc field of 5 kV/mm. As a comparison, a pure $BiFeO_3$ ceramic was prepared by a conventional ceramic technique and sintered at 775 °C for 2 h. Our study shows that the sintering temperature of pure $BiFeO_3$ is much lower than that of BFO-BT-Nd-x ceramics. The pure $BiFeO_3$ can be sintered at 775 °C/2 h; however, when sintering temperature increases above 775 °C (for 2 h), $BiFeO_3$ is melted.

The crystalline structure of the sintered samples was examined using X-ray diffraction (XRD) analysis with CuK_α radiation (SmartLab, Rigaku, Tokyo, Japan). The surface microstructures of the sintered samples were observed by scanning electron microscopy (SEM, FEI-Quanta 250, Oregon, USA). The average grain size was obtained by multiplying the average of grains by 1.56.[36,37] The bulk density ρ was measured by the Archimedes' method. The LCR meter (Agilent E4980A, Agilent Technologies Inc., Santa Clara, CA) and temperature controlled probe stage (Linkam TS1500E, Linkam Scientific Instruments Ltd., Guildford, UK) were used to measure the temperature dependence of relative permittivity ε_r of the sintered samples at 1 MHz. A precision materials measuring system (Premier II, Radiant Technologies Inc., Northford, USA) was used to measure the polarization hysteresis (P-E) loops and resistivity R at room temperature. The planar electromechanical coupling factor k_p was determined by the resonance method according to the IEEE Standards 176 using an impedance analyzer (Agilent 4294 A, Agilent Technologies Inc., Santa Clara, CA). The piezoelectric constant d_{33} was measured using a piezo-d_{33} meter (ZJ-3A, Institute of Acoustics, Chinese Academy of Sciences, Beijing, China). The magnetic hysteresis loops were measured using a magnetic measurement instrument (MPMS-XL-7, Quantum Design, San Diego, USA).

III. RESULTS AND DISCUSSIONS

Fig. 1 shows the XRD patterns of the BFO-BT-Nd-x ceramics sintered at 950 °C for 2 h, while the XRD patterns of the BFO-BT-Nd-0.05 ceramics sintered at different sintering temperatures T_s for 2 h are shown in Fig. 2. It has been known that the single-phase $BiFeO_3$ ceramic is difficult to synthesize because of its narrow temperature range of phase stabilization, resulting in some undesired impurity phases (e.g., $Bi_2Fe_4O_9$, $Bi_{25}FeO_{39}$, etc.).[9–11] However, from Figs. 1 and 2, all the BFO-BT-Nd-x ceramics exhibit the typical diffraction peaks of ABO_3 perovskite phase without an existence of any second phases. The results indicate that a homogeneous solid solution of BFO-BT-Nd-x could be formed after Nd and $BaTiO_3$ were added. Similar to $BiFeO_3$, the ceramic with x = 0 (i.e., without Nd doping) exhibits a rhombohedral symmetry. As x (i.e., the concentration of Nd)

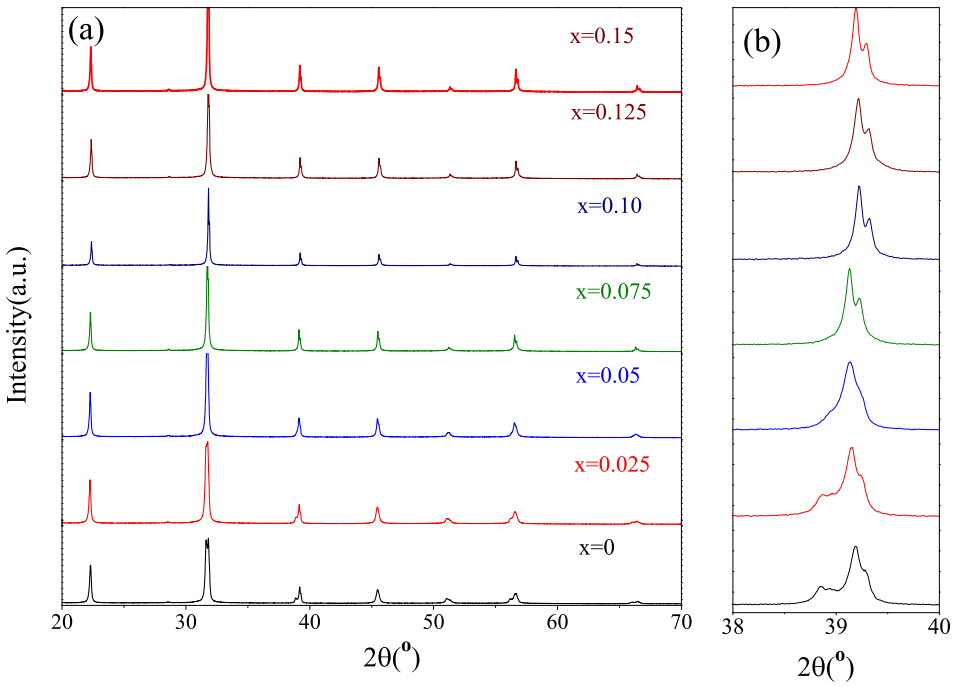

FIG. 1. XRD patterns of the BFO-BT-Nd-x ceramics sintered at 950 °C for 2 h.

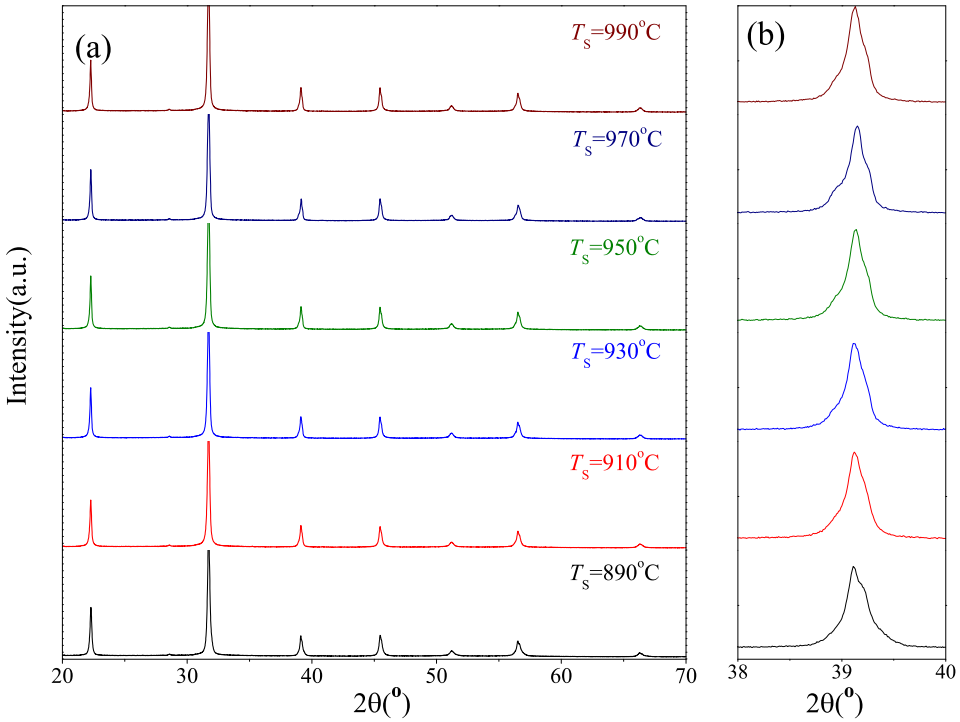

FIG. 2. XRD patterns of the BFO-BT-Nd-0.05 ceramics sintered at different T_s for 2 h.

increases, a monoclinic phase appears and grows continuously. At $x > 0.075$, the ceramic becomes a pure monoclinic phase (Fig. 1(b)). This suggests that a morphotropic phase boundary (MPB) of rhombohedral and monoclinic phases is formed at $x = 0.05$. The crystal structure transformation caused by the partial substitutions of analogous ions (e.g., La^{3+}, Sm^{3+}, Nd^{3+}, etc.) for Bi ions has been frequently observed in $BiFeO_3$-based materials.[15,17,32–34] For the present ceramics, the structure evolution may be ascribed to a chemical pressure related response induced by the partial substitution of Nd ions for Bi ions due to the smaller ionic radius of Nd^{3+} (0.131 nm) than that of Bi^{3+} (0.136 nm).[17] From Fig. 2, the BFO-BT-Nd-0.05 ceramics sintered at 890–930 °C have a rhombohedral structure. As T_s increases further to 990 °C, the ceramics are changed gradually into a coexistence of rhombohedral and monoclinic phases. This may be evidenced by the slight splitting of the diffraction peak near 39° as observed in the BFO-BT-Nd-0.05 ceramics with T_s increasing from 890 °C to 990 °C.

For all the ceramics, a general diffraction/reflectivity analysis program MAUD[38] was used to perform a full-pattern matching using the Rietveld method and refine the cell parameters. Based on the rhombohedral *R*3*c* and monoclinic *C*1*m*1 structures, the lattice parameters (*a*, *b*, *c*, and *β*) of the ceramics were refined using all the diffraction peaks shown in Figs. 1 and 2 by the Rietveld method. The composition and sintering temperature dependences of the lattice parameters (*a*, *b*, *c*, and *β*) and fitting parameters (R_{wp} and *S*) of the BFO-BT-Nd-x ceramics ($x = 0$, 0.025, 0.05, 0.075, 0.10, 0.125, and 0.15) sintered at 950 °C/2 h and the BFO-BT-Nd-0.05 ceramics sintered at 890–990 °C for 2 h are shown in Tables I and II, respectively. From Tables I and II, for all the refinement, the small values of the reliability R_{wp} of 7.43%–11.73% (<15%) and goodness-of-fit indicator *S* of 1.12–1.67 (<2) are obtained, suggesting a good agreement matching between the observed and calculated patterns.[38] That is, all diffraction peaks of the ceramics can be indexed and refined to the rhombohedral *R*3*c* and/or monoclinic

TABLE I. Composition dependences of the lattice parameters (*a*, *b*, *c*, and *β*) and fitting parameters (R_{wp} and *S*) of the BFO-BT-Nd-x ceramics ($x = 0$, 0.025, 0.05, 0.075, 0.10, 0.125, and 0.15) sintered at 950 °C/2 h. [the superscript "R" and "M" represent rhomhedral and monoclinic, respectively].

	Lattice parameters					R-factors (%)	
x	*a* (Å)	*b* (Å)	*c* (Å)	*β* (deg)	Weight (%)	R_{wp}	*S*
0	5.6275(5)	5.6275(5)	13.9049(5)	…	…	8.64	1.26
0.025	5.6273(5)	5.6273(5)	13.8783(4)	…	…	8.43	1.21
0.05	$5.6303(4)^R$	$5.6303(4)^R$	$13.8585(0)^R$	…	85.84^R	9.04	1.32
	$5.5512(1)^M$	$5.6914(2)^M$	$3.9949(7)^M$	84.2786(5)	14.16^M		
0.075	5.6285(0)	5.6343(3)	3.9859 (9)	89.9760(8)	…	8.55	1.22
0.1	5.6307(6)	5.6295(6)	3.9827(3)	89.9938(7)	…	7.97	1.14
0.125	5.6295(9)	5.6216(4)	3.9811(2)	90.0491(8)	…	7.43	1.12
0.15	5.6855(2)	5.6239(3)	3.9787(8)	91.9140(0)	…	9.57	1.39

TABLE II. Sintering temperature dependences of the lattice parameters (a, b, c, and β) and fitting parameters (R_{wp} and S) of the BFO-BT-Nd-0.05 ceramics sintered at 890–990 °C for 2 h. [the superscript "R" and "M" represent rhombhedral and monoclinic, respectively].

	Lattice parameters					R-factors (%)	
T_s (°C)	a (Å)	b (Å)	c (Å)	β (deg)	Weight (%)	R_{wp}	S
890	5.6379(9)	5.6379(9)	13.7831(0)	…	…	8.42	1.21
910	5.6315(4)	5.6315(4)	13.7939(4)	…	…	11.28	1.67
930	5.6296(3)	5.6296(3)	13.8413(6)	…	…	8.66	1.26
950	$5.6303(4)^R$	$5.6303(4)^R$	$13.8585(0)^R$	…	85.84^R	9.04	1.32
	$5.5512(1)^M$	$5.6914(2)^M$	$3.9949(7)^M$	84.2786(5)	14.16^M		
970	$5.6329(8)^R$	$5.6329(8)^R$	$13.8388(1)^R$	…	30.99^R	11.73	1.64
	$5.6398(5)^M$	$5.6303(6)^M$	$3.9930(5)^M$	90.0279(0)	69.01^M		
990	$5.6310(4)^R$	$5.6310(4)^R$	$13.8218(6)^R$	…	28.11^R	11.53	1.65
	$5.6404(5)^M$	$5.6333(2)^M$	$3.9895(2)^M$	89.8667(9)	71.89^M		

$C1m1$ structures by the Rietveld method. From Table I, for the BFO-BTO-Nd-x ceramics with rhombohedral symmetry, the observed lattice parameters a and c decreases from 5.6275 Å/13.9049 Å to 5.6273 Å/13.8783 Å with x increasing from 0 to 0.025; for the ceramics with monoclinic symmetry, as x increases from 0.075 to 0.15, the observed lattice parameters a and β increase from 5.6285 Å/89.9760° to 5.6855 Å/91.9140°, while the observed lattice parameters b and c decrease from 5.6343 Å/3.9859 Å to 5.6239 Å/3.9787 Å. A MPB could be identified in the BFO-BT-Nd-x ceramic with $x = 0.05$ within which the rhombohedral and monoclinic phases coexist with the relative concentration of 85.84% (R) and 14.16% (M), respectively. From Table II, the BFO-BTO-Nd-0.05 ceramics sintered at 890–930 °C for 2 h possess a rhombohedral symmetry; as T_s increases from 890 °C to 930 °C, the observed lattice parameter a decreases from 5.6379 Å to 5.6296 Å, while the observed lattice parameter c increases from 13.7831 Å to 13.8413 Å. At the T_s of 950–990 °C, the BFO-BT-Nd-0.05 ceramic is located at the coexistence zone of rhombohedral and monoclinic phases; with T_s increasing from 950 °C to 990 °C, the relative concentration of monoclinic phase increases from 14.16% to 71.89%.

Fig. 3 shows the SEM graphs of the surface microstructure of the BFO-BT-Nd-x ceramics with $x = 0$, 0.05, 0.10, and 0.15 sintered at 950 °C for 2 h. It can be seen that all the ceramics are dense without pores (Fig. 3). From Fig. 3(a), for the BFO-BT-Nd-0 ceramic, the grains have an average grain size of about 6.58 μm. After the partial substitution of Nd^{3+} for Bi^{3+}, the grain size of the ceramics gradually

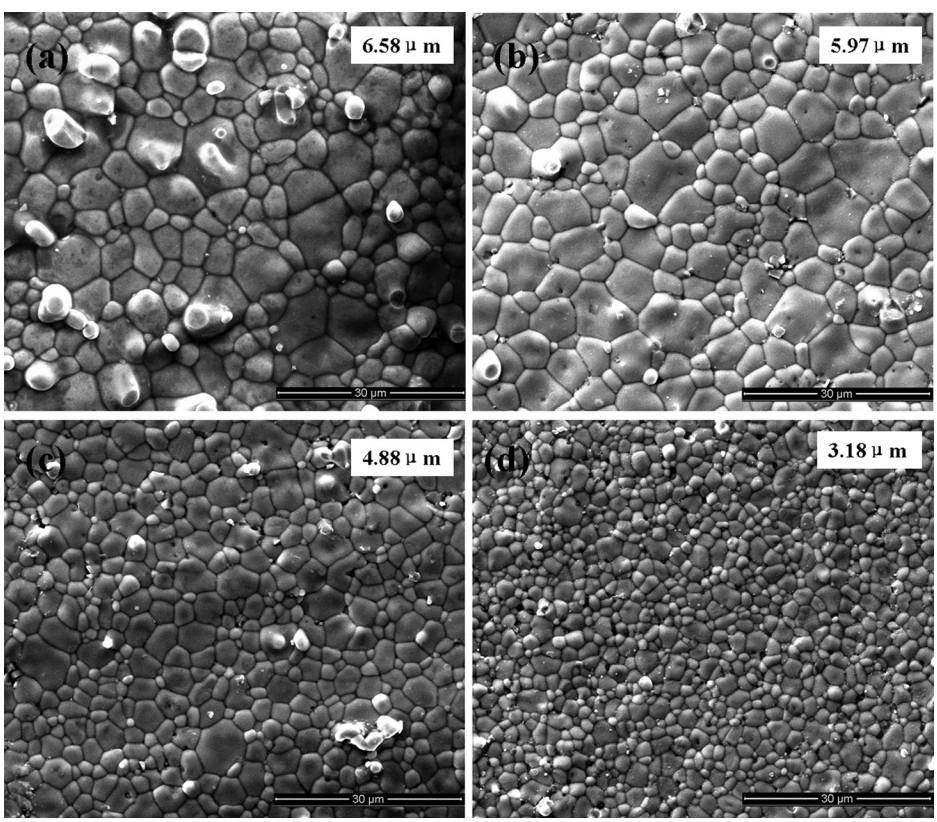

FIG. 3. SEM graphs of the surface microstructure of the BFO-BT-Nd-x ceramics with $x = 0$ (a), 0.05 (b), 0.10 (c), and 0.15 (d) sintered at 950 °C for 2 h.

becomes smaller and the average grain sizes of the ceramics with x = 0.05, 0.10, and 0.15 are about 5.97 μm, 4.88 μm and 3.18 μm, respectively, suggesting that the Nd doping has an obvious effect on the inhibition of grain growth. It has been known that rare earth ions are usually considered as grain growth inhibitor in perovskites because of their relatively low diffusivity.[15] This leads to the decrease in grain size of the ceramics after the Nd doping. Similar suppressed effect of grain growth induced by rare earth ions doping has been observed in La- and Sm-modified $BiFeO_3$ ceramics.[15,32]

Fig. 4 shows the SEM graphs of the surface microstructure of the BFO-BT-Nd-0.05 ceramics sintered at 890 °C, 910 °C, 930 °C, 950 °C, 970 °C, and 990 °C for 2 h, while the grain size distributions of the ceramics with x = 0.05 sintered at 890 °C, 910 °C, 930 °C, 950 °C, 970 °C, and 990 °C are shown in Fig. 5. It can be seen that the sintering temperature has a very important influence on the microstructure of the ceramic with x = 0.05 (Fig. 4). From Fig. 4(a), the BFO-BT-Nd-0.05 ceramic sintered at 890 °C for 2 h exhibits a very uniform and loose structure with a large amount of pores and ambiguous grain boundary. The average grain size of the ceramic with x = 0.05 sintered at 890 °C for 2 h is about 1.83 μm. Clearly, the T_s of 890 °C is not high enough for sintering and densification of the ceramic. As T_s increases from 910 °C to 990 °C, the ceramics are well crystallized and become gradually dense; and distinct grains and clear grain boundaries are observed in the ceramic with x = 0.05 sintered at 930–990 °C (Figs. 4(c)–4(f)). The increase in T_s leads to the significant increase in the grain size of the ceramics. The average grain size values of the ceramic with x = 0.05 sintered at 910 °C, 930 °C, 950 °C, 970 °C, and 990 °C for 2 h are about 3.53 μm, 4.87 μm, 5.93 μm, 7.85 μm, and 9.39 μm, respectively. From Fig. 5(a), for the ceramic with x = 0.05 sintered at 890 °C for 2 h, most of grains (~90%) exhibit a range of average grain size between 0.3 and 3.0 μm and the size distribution is pseudo-symmetric, suggesting that the grain sizes are relatively uniform. However, the observed average grain size distribution becomes gradually wider and much asymmetric with T_s increasing, showing that large and small grains coexist in the ceramic with x = 0.05 (Figs. 5(b)–5(f)). This coexistence of large and small grains in the present ceramics sintered at high temperatures has been observed in piezoelectric ceramics.[39–41]

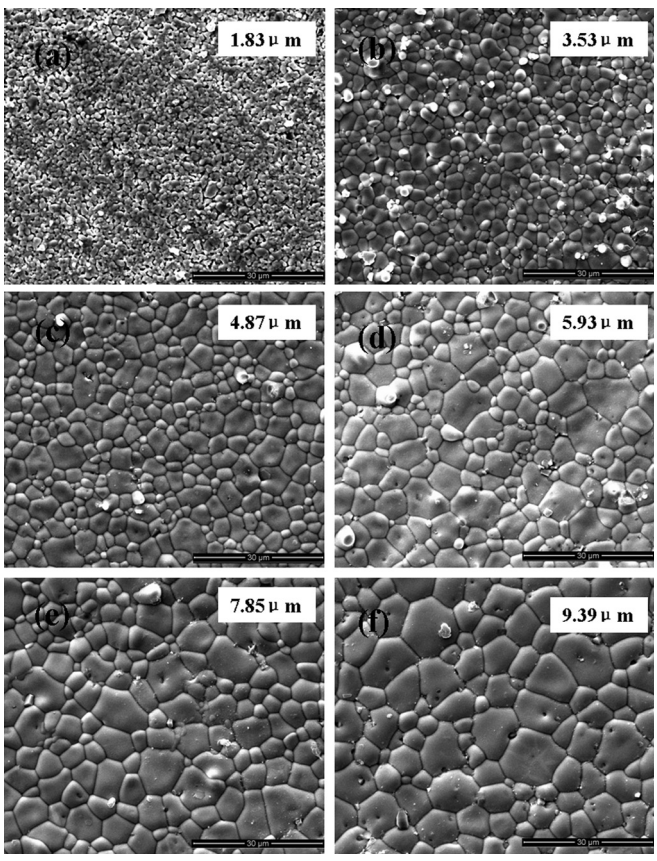

FIG. 4. SEM graphs of the surface microstructure of the BFO-BT-Nd-0.05 ceramics sintered at (a) 890 °C, (b)910 °C, (c) 930 °C, (d) 950 °C, (e) 970 °C, and (f) 990 °C for 2 h.

Fig. 6(a) shows the compositional dependence of the relative density ρ_r of the BFO-BT-Nd-x ceramics sintered at 950 °C for 2 h, while the ρ_r of the BFO-BT-Nd-0.05 ceramics as a function of T_s is shown in Fig. 6(b). From Fig. 6(a), the observed ρ_r of the BFO-BT-Nd-x ceramics with x = 0 has a high ρ_r of 94.3%. After the addition of 2.50–7.50 mol. % Nd, the observed ρ_r increases significantly to 97.9% and then decreases slightly to 95.2% with x further increasing to 0.15. From Fig. 6(b), the T_s has a significant influence on the ρ_r of the BFO-BT-Nd-0.05 ceramics. The BFO-BT-Nd-0.05 ceramic sintered at 890 °C for 2 h has a relatively low ρ_r value of 86.0%. As T_s increases to 910 °C, the observed ρ_r of the ceramic increases significantly to 96.0%. As T_s further increases to 930–990 °C, the observed ρ_r of the BFO-BT-Nd-0.05 ceramic exhibits a small fluctuation of 97.3–97.7% (Fig. 6(b)). These results show that as compared to other perovskite ceramics,[1–3,42] the BFO-BT-Nd-x ceramics can be well densified at the wide range of very low sintering temperatures of 910–990 °C.

Figs. 7(a) and 7(b) show the dependences of the resistivity R of the BFO-BT-Nd-x ceramics with x = 0, 0.05, 0.10, and 0.15 sintered at 950 °C for 2 h and the BFO-BT-Nd-0.05 ceramics sintered at 890 °C, 950 °C, and 990 °C for 2 h on the electric field E, respectively. As a comparison, a pure $BiFeO_3$ ceramic was sintered at 775 °C for 2 h, and its variation of R with E is also plotted in Fig. 7(a). It can be seen that the pure $BiFeO_3$ ceramic exhibits a very low R value of 2.27×10^7 Ω·cm (under 3.0 kV/mm). This is due to the reduction of Fe ions from Fe^{3+} to Fe^{2+} during sintering and the formation of oxygen vacancies $V_O^{\bullet\bullet}$ for charge compensation.[10–12] However, from Fig. 7, all the BFO-BT-Nd-x ceramics sintered at 890–990 °C exhibit the significant improved R values of $3.01 \times 10^9 - 1.67 \times 10^{10}$ Ω·cm under the electric field of 3 kV/mm, showing that the introduction of $BaTiO_3$ and MnO_2 into $BiFeO_3$ could greatly improve the electric insulation of the ceramics. The partial substitutions of Fe^{3+} by Mn^{4+} and Ti^{4+} lead to the significant suppression of the formation of $Fe_{Fe3+}^{2+\prime}$ and $V_O^{\bullet\bullet}$.[11,12,21] As a result, the improved resistivity of the BFO-BT-Nd-x ceramics sintered at 890–990 °C is obtained. Similar enhancement in the electric insulation induced by Mn and/or Ti doping has been observed in modified $BiFeO_3$ materials.[12,21,30,31] From Fig.

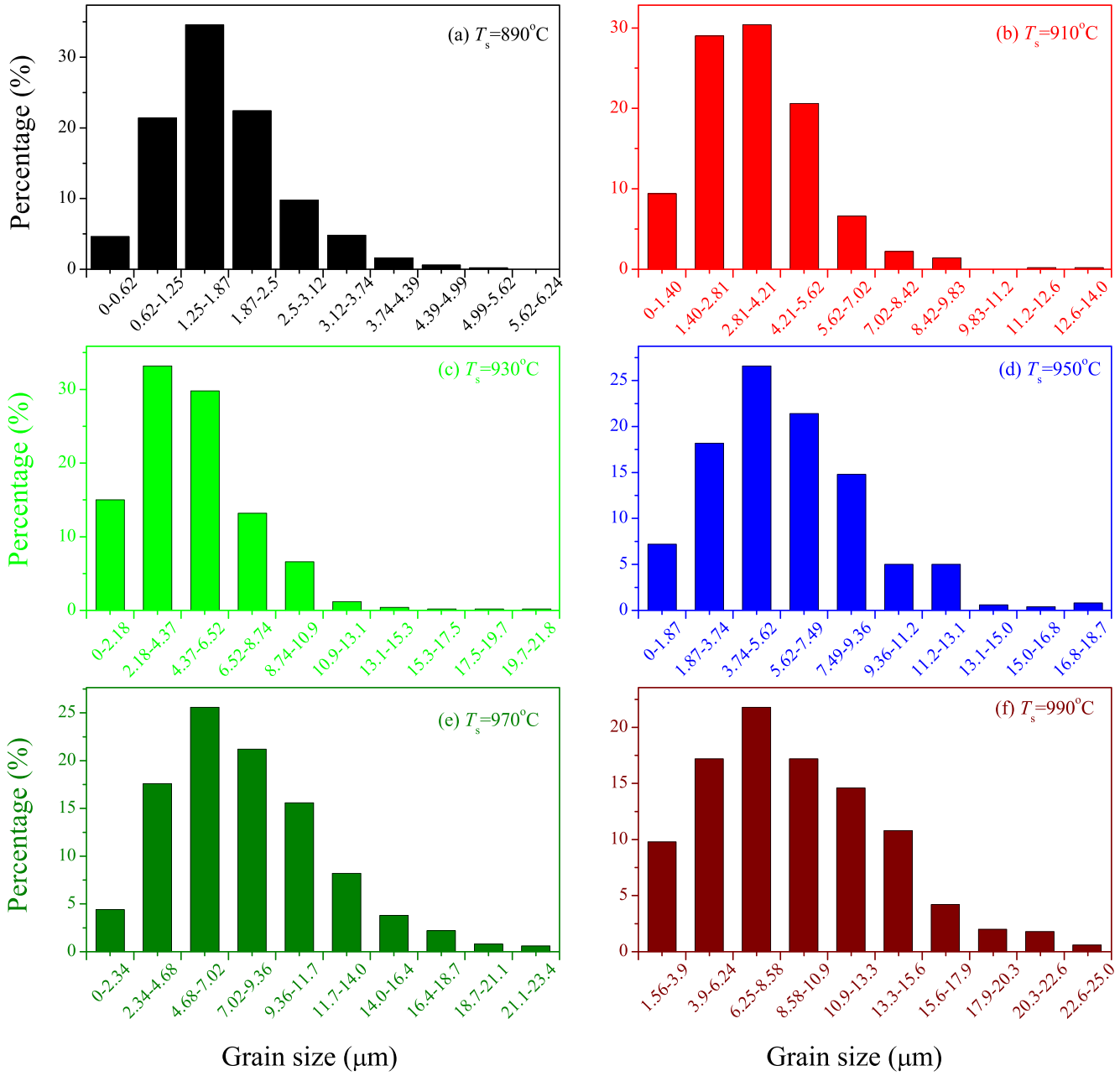

FIG. 5. Grain size distribution of the BFO-BT-Nd-0.05 ceramics sintered at different T_s for 2 h.

7(a), Nd doping slightly improves the electric insulation of the ceramics. This may be ascribed to the suppression of the possible volatility of Bi^{3+} at high sintering temperatures after the addition of Nd^{3+}.

Figs. 8(a) and 9(a) show the *P-E* loops of the BFO-BT-Nd-x ceramics sintered at 950 °C for 2 h and the BFO-BT-Nd-0.05 ceramics sintered at different T_s, while the composition and sintering temperature dependences of the remnant polarization P_r and coercive filed E_c of the BFO-BT-Nd-x ceramics sintered at 950 °C for 2 h and the BFO-BT-Nd-0.05 ceramics sintered at different T_s are shown in Figs. 8(b) and 9(b), respectively. Because of much better electric insulation than the pure $BiFeO_3$ ceramic (Fig. 7), all the ceramics sintered at 890–990 °C possess typical and saturated *P-E* loops (Figs. 8(a) and 9(a)). From Figs. 8(a) and 8(b), the addition of a small amount of Nd ($x \leq 0.05$) enhances significantly the ferroelectricity of the ceramics, while excess Nd doping ($x \geq 0.10$) degrades greatly the ferroelectricity of the ceramics. For the ceramics with a low level of Nd doping ($x = 0$–0.05), well saturated and developed *P-E* loops are observed and the increased P_r values from 10.0 $\mu C/cm^2$ to 16.5 $\mu C/cm^2$ are obtained with x increasing from 0 to 0.05. However, with the addition of excess Nd ($x = 0.075$–0.15), the observed P_r decreases steeply from 8.15 $\mu C/cm^2$ to 0.85 $\mu C/cm^2$ with x increasing from 0.075 to 0.15. Besides, slim and slanted *P-E* loops are also observed in the ceramics with high Nd level ($x = 0.075$–0.15). This may be attributed to the higher disorder in the structure induced by the addition of excess Nd^{3+}.[43] Like P_r, similar variation of E_c with x is observed and the maximum E_c value of 4.37 kV/mm is obtained at $x = 0.05$. These results suggest that a low doping level of Nd ($x = 0$–0.05) can enhance effectively the

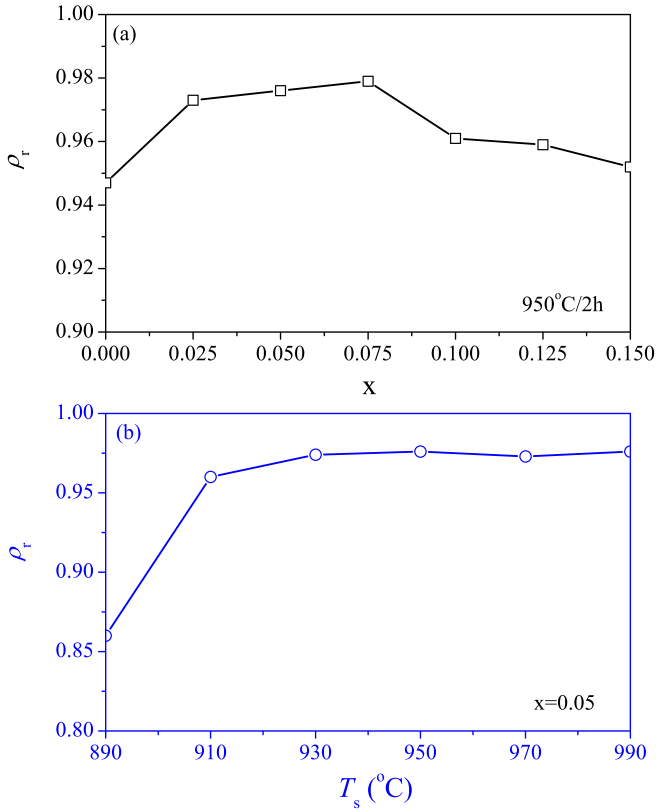

FIG. 6. (a) Dependence of ρ_r of the BFO-BT-Nd-x ceramics sintered at 950 °C for 2 h on x; (b) Variation of ρ_r of the BFO-BT-Nd-0.05 ceramics with T_s.

ferroelectricity of the BFO-BT-Nd-x ceramics. It has been known that for conventional perovskite ferroelectrics, the charge transfer from the oxygen to the unoccupied transition metal *d* orbital can stabilize the ferroelectric distortion. In spite of the partial substitution of a small amount of Nd^{3+}

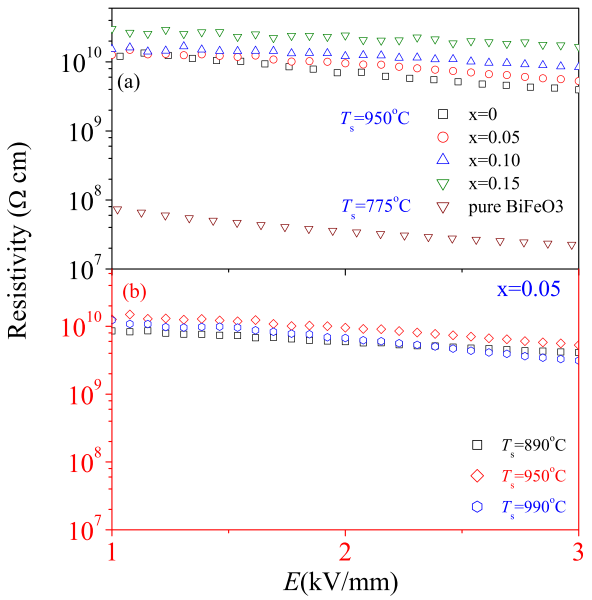

FIG. 7. Dependence of *R* of (a) the BFO-BT-Nd-x ceramics with x = 0, 0.05, 0.10, and 0.15 sintered at 950 °C for 2 h and the $BiFeO_3$ ceramic sintered at 775 °C for 2 h and (b) the BFO-BT-Nd-0.05 ceramics sintered at 890 °C, 950 °C, and 990 °C for 2 h on the electric field *E*.

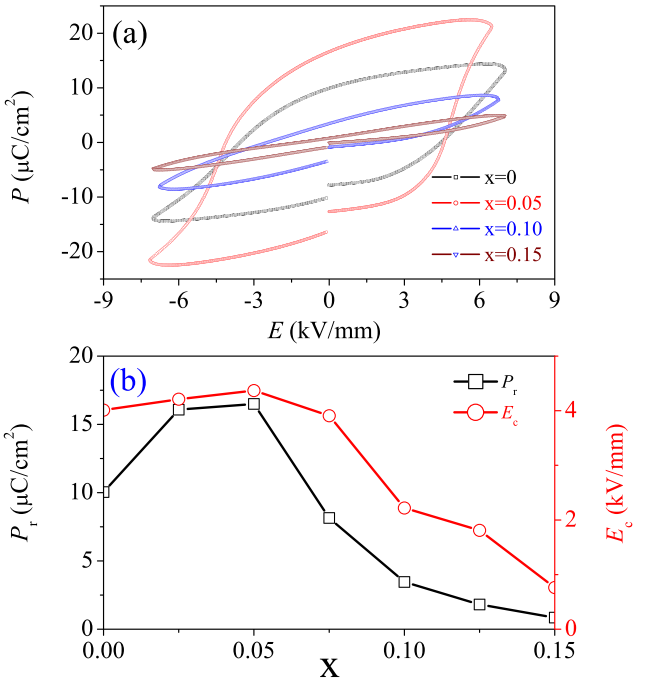

FIG. 8. (a) *P-E* loops of the BFO-BT-Nd-x ceramics sintered at 950 °C for 2 h; and (b) Variations of P_r and E_c of the BT-BFO-Nd-x ceramics sintered at 950 °C for 2 h with x.

($x \leq 0.05$) for Bi^{3+}, a lone s^2 of electrons of Bi^{3+} can hybridize with an empty p orbital of Bi^{3+} or O^{2-} to form a localized lobe, which leads to the noncentrosymmetric distortion and thus enhances the ferroelectricity of the materials.[33] However, the introduction of excess Nd ($x \geq 0.075$) may weaken the stereochemical activity of the Bi lone electron pair.[33] As a

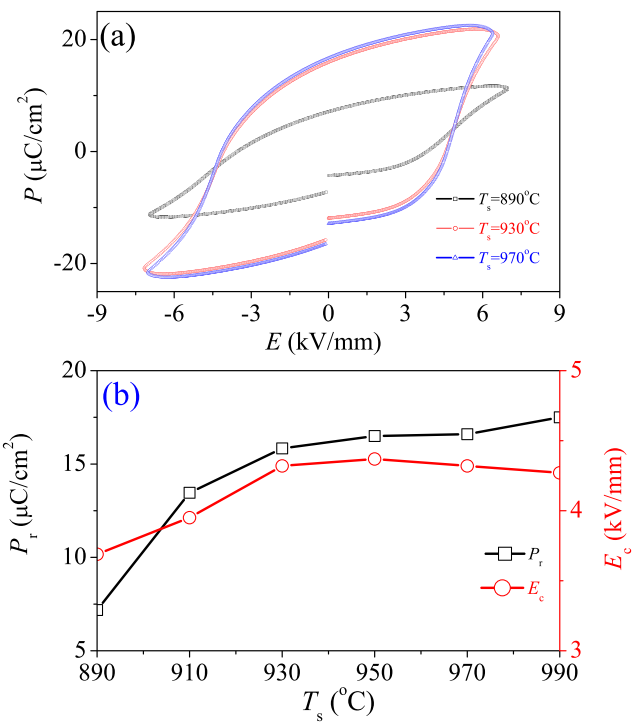

FIGS. 9. (a) *P-E* loops of the BFO-BT-Nd-0.05 ceramics sintered at different T_s for 2 h; and (b) Variations of P_r and E_c of the BFO-BT-Nd-0.05 ceramics for 2 h with T_s.

result, the degraded ferroelectricity of the ceramics is obtained in the ceramics with high Nd levels. From Fig. 9(b), as T_s increases from 890 °C to 990 °C, the observed P_r increases greatly from 7.18 μC/cm^2 to 17.5 μC/cm^2, while the observed E_c increases slightly from 3.69 kV/mm to 4.27 kV/mm. Clearly, the sintering temperature has an important influence on the ferroelectricity of the BFO-BT-Nd-0.05 ceramics. From Fig. 4, the grain size of the ceramics increases with the sintering temperature. Therefore, it may be concluded that there is a positive correlation between the ferroelectricity and grain size of the BFO-BT-Nd-0.05 ceramics. That is, the bigger the grains of the ceramics, the larger the polarization of the ceramics. This may be ascribed to the easier polarization reversal process of ferroelectric domain in larger grains than in smaller grains.[44–47] Similar grain size effect on ferroelectricity has been frequently observed in the perovskite $BaTiO_3$-[44] and $Pb(Ti,Zr)O_3$-based ceramics.[45]

Fig. 10(a) shows the temperature dependence of relative permittivity ε_r and loss tangent $\tan\delta$ at 1 MHz for the BFO-BT-Nd-x ceramics sintered at 950 °C for 2 h, while the variation of Curie temperature T_C of the BFO-BT-Nd-x ceramics sintered at 950 °C for 2 h with x is shown in Fig. 10(b). All the ceramics (x = 0–0.15) exhibit only a dielectric peak (Fig. 10(a)). As x increases, the phase transition peaks of the ceramics become gradually broad. This suggests that the partial substitution of Nd^{3+} for Bi^{3+} induces a diffusive phase transition in the ceramics with high level of Nd^{3+}. Due to small difference of ionic radius between Bi^{3+} and Nd^{3+}, the addition of Nd^{3+} may lead to the increment in the disorder degree of A-site ions and the local compositional fluctuation. Consequently, a diffusive phase transition is observed in the ceramics with high Nd^{3+} levels. From Fig. 10(b), after the partial substitution of Nd^{3+} for Bi^{3+}, the observed T_C decreases greatly from 655 °C to 391 °C. The decrease in T_C may be due to the softness of the short-range repulsion force against the ferroelectric ordering.[48] Similar effect of ion substitution on phase transition temperature has been observed in Sm-modified $BiFeO_3$ ceramics.[49]

Fig. 11(a) shows the temperature dependence of ε_r and $\tan\delta$ at 1 MHz for the BFO-BT-Nd-0.05 ceramics sintered at different T_s for 2 h, while the variation of T_C of the BFO-BT-Nd-0.05 ceramics with T_s is shown in Fig. 11(b). From Fig. 11(a), all the BFO-BT-Nd-0.05 ceramics sintered at 890–990 °C exhibit a ferroelectric-paraelectric phase transition peak at T_C. The ceramic sintered at 890 °C exhibits a broad peak at T_C. However, as T_s increases, the dielectric peak becomes sharper and much intense, which corresponds to the increase in grain size induced by the increase in T_s. In general, the ceramics with large grains exhibit sharper and more intense phase transition peaks than those with small grains. This phenomenon has been frequently reported in perovskite ferroelectrics.[44,50–52] From Fig. 11(b), the observed T_C shifts to low temperature (from 502 °C to 473 °C) with T_s increasing from 890 °C to 990 °C. From Figs. 4 and 11, the BFO-BT-Nd-0.05 ceramics with large

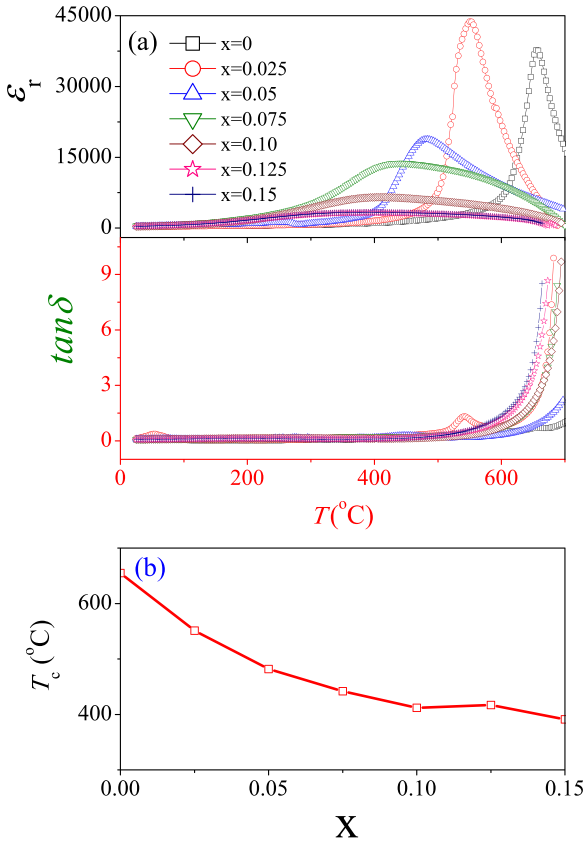

FIG. 10. (a) Temperature dependences of ε_r and $\tan\delta$ at 1 MHz for the BFO-BT-Nd-x ceramics sintered at 950 °C for 2 h; (b) Compositional dependence of T_C of the BFO-BT-Nd-x ceramics sintered at 950 °C for 2 h on x.

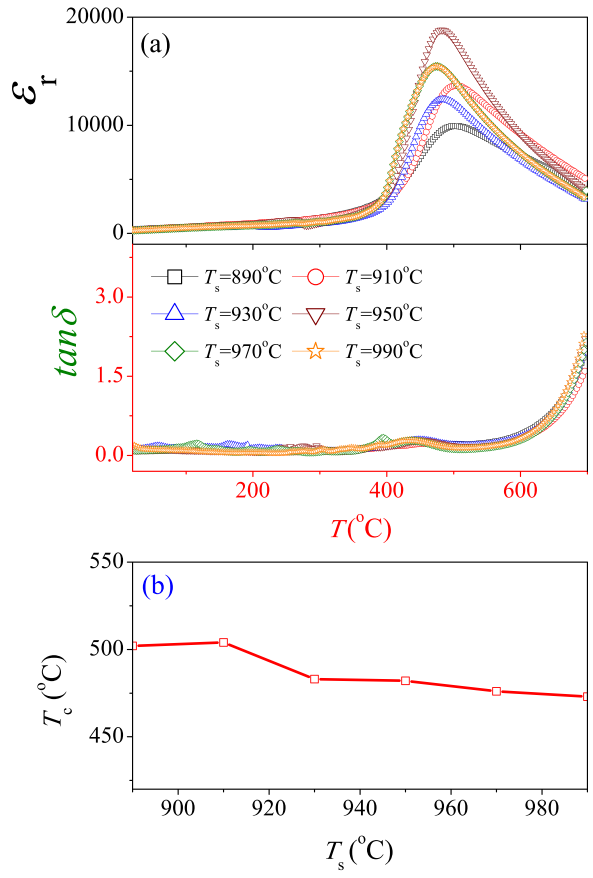

FIG. 11. (a) Temperature dependences of ε_r and $\tan\delta$ at 1 MHz for the BFO-BT-Nd-0.05 ceramics sintered at different sintering temperature T_s for 2 h; (c) Variation of T_C of the BFO-BT-Nd-0.05 ceramics with T_s.

grains exhibit lower T_C than those with small grains. This negative correlation between Curie temperature and grain size has been frequently reported and well corresponds to the results of some investigations.[44,52–54] It is also noted from Fig. 2 that the diffraction peaks shift slightly to higher diffraction angles with grain size (sintering temperature) increasing. This suggests that there is shrinkage of cell volumes in the coarse-grained ceramics. This cell volume effect may lead to the decrease in the T_C.[44] However, the exact reason for the decrease in the T_C with grain size increasing in the present ceramics is still unclear.

The composition dependences of piezoelectric constant d_{33}, planar electromechanical coupling factor k_p, relative permittivity ε_r, and loss tangent $\tan\delta$ for the BFO-BT-Nd-x ceramics sintered at 950 °C for 2 h are shown in Fig. 12, while the variations of d_{33}, k_p, ε_r, and $\tan\delta$ of BFO-BT-Nd-0.05 ceramics sintered for 2 h with T_s are shown in Fig. 13. For the BFO-BT-Nd-x ceramics sintered at 950 °C for 2 h, the observed d_{33} increases from 90 pC/N to 113 pC/N with x increasing from 0 to 0.05 and then decreases greatly to 4 pC/N with x increasing to 0.15. The observed k_p gives large values of 28.0%–32.4% at x = 0–0.05 and then decreases quickly to 8.5% with x increasing to 0.15. Clearly, the substitution of 5 mol. % Nd^{3+} for Bi^{3+} can enhance the piezoelectric properties, which should be attributed to the improved polarization and formation of the MPB in the Nd-doped ceramics. However, excess Nd^{3+} (x = 0.075–0.15) degrades significantly the piezoelectric properties of the ceramics with x = 0.075–0.15 because of the very weak ferroelectricity of the ceramics (Fig. 8). The observed ε_r and $\tan\delta$ exhibit similar compositional dependences and give the maximum values of 559 and 4.75% at x = 0.05 (Fig. 12(b)), respectively. From Fig. 13, the observed d_{33}/k_p of the BFO-BT-Nd-0.05 ceramics sintered for 2 h increase monotonously from 40 pC/N/14.8% to 121 pC/N/29.4% with T_s increasing from 890 °C to 990 °C. These variations of d_{33} and k_p with T_s are consistent with that of the polarization of the ceramics with T_s. From Figs. 4 and 9(b), as T_s increases, the ferroelectricity of the ceramics is enhanced; as a result, the piezoelectricity of the ceramics is improved with T_s (grain size) increasing. The observed ε_r increases linearly from 451 to 561 with T_s increasing from 890 °C to 950 °C and then remains a large value of 560 at T_s = 950–990 °C. The observed $\tan\delta$ decreases from 8.27% to 4.43% with T_s increasing 890 °C to 910 °C and then exhibits the relatively small values of 4.43%–4.75% at T_s = 910–990 °C.

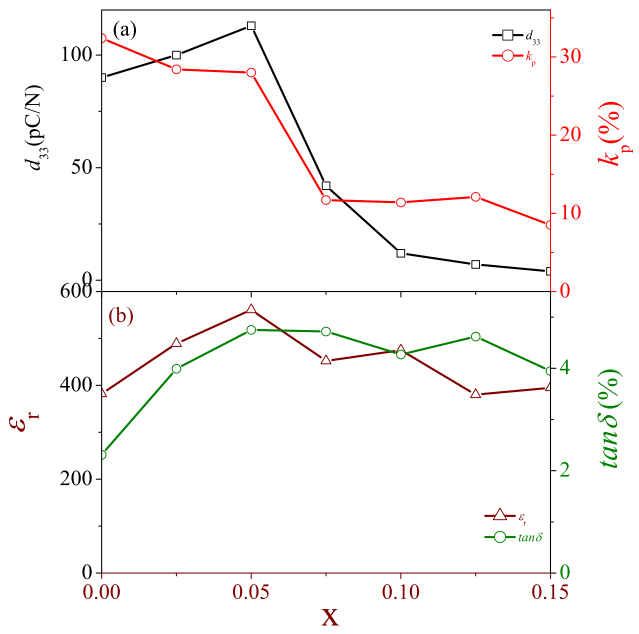

FIG. 12. Composition dependence of d_{33}, k_p, ε_r, and $\tan\delta$ for the BFO-BT-Nd-x ceramics sintered at 950 °C for 2 h.

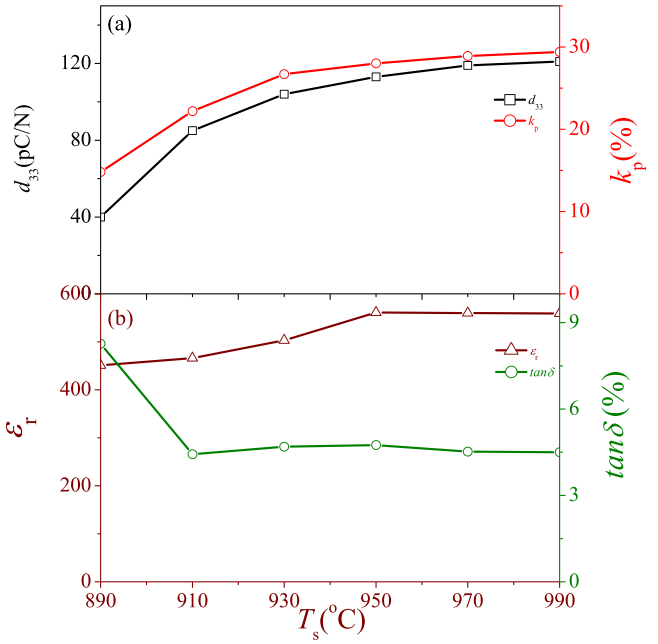

FIG. 13. Variations of d_{33}, k_p, ε_r and $\tan\delta$ for the BFO-BT-Nd-0.05 ceramics sintered for 2 h with T_s.

The *M-H* hysteresis loops of the BFO-BT-Nd-x ceramics with x = 0, 0.05, 0.10, and 0.15 sintered at 950 °C for 2 h are shown in Fig. 14(a), while Fig. 14(b) shows the *M-H* hysteresis loops of the BFO-BT-Nd-0.05 ceramics sintered at 890 °C, 950 °C, and 990 °C for 2 h. From Fig. 14, all the BFO-BT-Nd-x ceramics exhibit the typical magnetization hysteresis loops, suggesting that the ceramics possess simultaneously ferromagnetism and ferroelectricity (Figs. 8, 9, and 14). From Fig. 14(a), the ceramic with x = 0 exhibits the weak ferromagnetism and the observed saturation magnetization M_s, remnant magnetization M_r, and coercive field H_c are 0.314 emu/g, 0.054 emu/g, and 2.31 kOe, respectively. Nd^{3+} doping improves greatly the ferromagnetism of the ceramics. After the addition of 15 mol. % Nd^{3+}, the remnant magnetization of the ceramics is increased by ~320% (from $M_r \sim 0.054$ emu/g at x = 0 to $M_r \sim 0.226$ emu/g at x = 0.15). The ceramics with x = 0.05, 0.10, and 0.15 exhibit the M_s values of 0.495/0.632/0.765 emu/g, M_r values of 0.127/0.176/0.226 emu/g, and H_c values of 3.54/3.56/4.26 kOe, respectively. As known, the pure BFO is antiferromagnetic with a G-type structure and the Fe^{3+} magnetic moments ordering forms a long-rang cycloid and thus leads to zero net magnetization.[55] As a comparison, the *M-H* hysteresis loop of pure $BiFeO_3$ was measured and the result is shown in

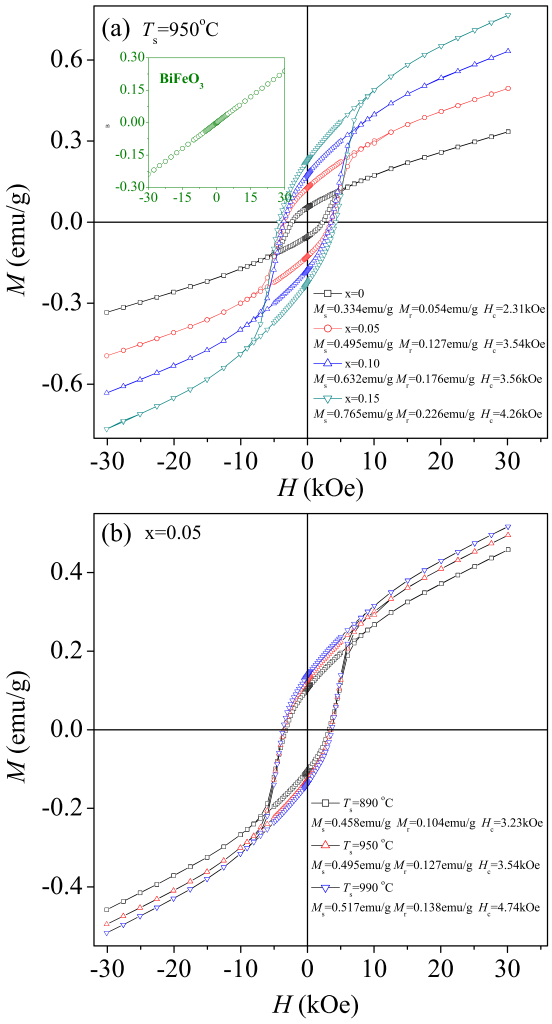

FIG. 14. (a) *M-H* loops of the BFO-BT-Nd-x ceramics sintered at 950 °C for 2 h (The inset is *M-H* hysteresis loop of $BiFeO_3$ ceramic sintered 775 °C for 2 h); (b) *M-H* loops of the BFO-BT-Nd-0.05 ceramics sintered at different temperature for 2 h.

the inset of Fig. 14(a). It can be seen that a linear dependence of magnetization on magnetic field is observed, showing the antiferromagnetic characteristic of $BiFeO_3$, which is consistent with the previous reports.[22,32,33] In general, the addition of rare earth ions and other ABO_3-type compounds induces the weak ferromagnetism or improves the magnetism of the BFO-based materials.[15,17,21–23] For the BFO-BT-Nd-0 ceramic, after the addition of 25 mol. % $BaTiO_3$ and 1 mol. % MnO_2 to $BiFeO_3$, the spatially modulated spin order in the ceramics with $x = 0$ is suppressed. This releases the locked magnetization and leads to nonlinear *M-H* hysteresis loops with weak ferromagnetism. However, the M_r of the BFO-BT-Nd-0 ceramic is very small (~0.054 emu/g). From Fig. 14(a), the partial substitution of Nd^{3+} for Bi^{3+} in the $0.75BiFeO_3$–$0.25BaTiO_3 + 1$ mol% MnO_2 plays an important role in enhancing the ferromagnetism of the materials. The addition of a small amount of Nd^{3+} ($x < 0.05$) suppresses the space-modulated spin structure of the $BiFeO_3$ matrix, while the doping of high Nd^{3+} levels ($x \geq 0.05$) results in a structural phase transformation, leading to the further destruction of the space-modulated spin structure. These release the latent magnetization locked within the cycloid and thus a significantly enhanced M_r is observed in the Nd-modified ceramics. Similar enhancing ferromagnetism effect induced by rare earth ions or structural phase transformation has been frequently reported in Nd-, La-, and Sm-doped $BiFeO_3$ materials.[32–35] From Fig. 14(b), the increase in T_s leads to the slight improvement in the ferromagnetism of the ceramic with $x = 0.05$. The observed M_s, M_r, and H_c increase slightly from 0.458 emu/g, 0.104 emu/g, and 3.23 kOe to 0.517 emu/g, 0.138 emu/g, and 4.74 kOe with T_s increasing from 890 °C to 990 °C. The improvement in the ferromagnetism induced by the increase in T_s may be attributed to the decrement in the structural symmetry of the ceramics. From Fig. 2, as T_s increases, the ceramics are transformed gradually from rhombohedral phase to a coexistence of rhombohedral and monoclinic phases. This may cause the formation of a more imperfect antiferromagnetic ordering at higher T_s. As a result, the ferromagnetism of the ceramics is improved by the increase in T_s. Similar effect of the crystal symmetry on ferromagnetism has been observed in $BiFeO_3$-$SrTiO_3$ and $BiFeO_3$-$BaTiO_3$ materials.[33,35]

IV. CONCLUSIONS

Lead-free multiferroic ceramics of $0.75Bi_{1-x}Nd_xFeO_3 - 0.25BaTiO_3 + 1$ mol. % MnO_2 have been fabricated by a solid state reaction method. The phase structure, ferroelectric, piezoelectric, and ferromagnetic properties of the ceramics have been studied. The Nd-modified $BiFeO_3$-$BaTiO_3$ ceramics with a pure perovskite structure can be well sintered at the very low and wide range of sintering temperatures (910–990 °C), which exhibit good electric insulation and high densification. After the addition of a small amount of Nd^{3+} ($x \leq 0.05$), the ferroelectric and piezoelectric properties of the ceramics are improved and the optimum ferroelectricity ($P_r = 16.5\ \mu C/cm^2$) and piezoelectricity ($d_{33} = 113$ pC/N) are observed at $x = 0.05$, respectively, while excess Nd ($x = 0.075$–0.15) degrades greatly the ferroelectric and piezoelectric properties. As the Nd^{3+} level increases, the ferroelectric-paraelectric phase transition becomes gradually diffusive. The doping of Nd enhances significantly the ferromagnetic properties of the ceramics. The remnant magnetization M_r is increased greatly by ~320% with x increasing from 0 to 0.15. The study shows that the sintering temperature plays an important role in enhancing the ferroelectric, piezoelectric, and ferromagnetic properties of the ceramics. The increase in the sintering temperature promotes the grain growth, causes good densification and improves the ferroelectric, piezoelectric, and ferromagnetic properties of the ceramics. The ceramic with $x = 0.05$ sintered at 950 °C possesses the improved ferroelectric, piezoelectric, and ferromagnetic properties with P_r of 16.5 $\mu C/cm^2$, d_{33} of 113 pC/N, M_r of 0.127 emu/g, large R of 5×10^9 Ω·cm, and high T_C of 482 °C, indicating that the ceramic is an interesting candidate for room-temperature multiferroic materials and high temperature piezoelectric materials.

ACKNOWLEDGMENTS

This work was supported by the projects of Science and Technology Bureau of Sichuan Province (2010JQ0046) and Sichuan Normal University.

[1]W. Liu and X. Ren, Phys. Rev. Lett. **103**, 257602 (2009).
[2]S. T. Zhang, B. Yang, and W. W. Cao, Acta. Mater. **60**, 469 (2012).
[3]D. J. Shin and J. H. Koh, J. Alloys Compd. **555**, 390 (2013).
[4]Q. He, C. H. Yeh, J. C. Yang, G. Singh-Bhalla, C. W. Liang, P. W. Chiu, G. Catalan, L. W. Martin, Y. H. Chu, J. F. Scott, and R. Ramesh, Phys. Rev. Lett. **108**, 067203 (2012).
[5]J. H. Lee, M. A. Oak, H. J. Choi, J. Y. Son, and H. M. Jang, J. Mater. Chem. **22**, 1667 (2012).
[6]T. R. Paudel, S. S. Jaswal, and E. Y. Tsymbal, Phys. Rev. B **85**, 104409 (2012).
[7]S. Goswami, D. Bhattacharya, P. Choudhury, B. Ouladdiaf, and T. Chatterji, Appl. Phys. Lett. **99**, 073106 (2011).
[8]F. Azough, R. Freer, M. Thrall, R. Cernik, F. Tuna, and D. Collison, J. Eur. Ceram. Soc. **30**, 727 (2010).
[9]M. M. Kumar, V. R. Palker, K. Srinvivas, and S. V. Suryanarayana, Appl. Phys. Lett. **76**, 2764 (2000).
[10]A. K. Pradhan, K. Zhang, D. Hunter, J. B. Dadson, and G. B. Loutts, J. Appl. Phys. **97**, 093903 (2005).
[11]S. K. Pradhan and B. K. Roul, Phys. B **406**, 3313 (2011).
[12]T. Kawae, Y. Terauchi, H. Tsuda, M. Kumeda, and A. Morimoto, Appl. Phys. Lett. **94**, 112904 (2009).
[13]A. Sagdeo, P. Mondal, A. Upadhyay, A. K. Sinha, A. K. Srivastava, S. M. Gupta, P. Chowdhury, T. Ganguli, and S. K. Deb, Solid State Sci. **18**, 1 (2013).
[14]Y. P. Wang, L. Zhou, M. F. Zhang, X. Y. Chen, J. M. Liu, and Z. G. Liu, Appl. Phys. Lett. **84**, 1731 (2004).
[15]Q. Zhang, X. H. Zhu, Y. H. Xu, H. B. Gao, Y. J. Xiao, D. Y. Liang, J. L. Zhu, J. G. Zhu, and D. Q. Xiao, J. Alloys Compd. **546**, 57 (2013).
[16]X. M. Chen, J. L. Wang, G. L. Yuan, D. Wu, J. M. Liu, J. Yin, and Z. G. Liu, J. Alloys Compd. **541**, 173 (2012).
[17]Y. J. Wu, X. K. Chen, J. Zhang, and X. J. Chen, J. Appl. Phys. **111**, 053927 (2012).
[18]Z. Y. Cen, C. R. Zhou, H. B. Yang, Q. Zhou, W. Z. Li, C. L. Yan, L. Cao, J. Song, and L. Peng, J. Am. Ceram. Soc. **96**, 2252 (2013).
[19]D. Varshney, A. Kumar, and K. Verma, J. Alloys Compd. **509**, 8421 (2011).
[20]T. H. Wang, C. S. Tu, Y. Ding, T. C. Lin, C. S. Ku, W. C. Yang, H. H. Yu, K. T. Wu, Y. D. Yao, and H. Y. Lee, Curr. Appl. Phys. **11**, S240 (2011).
[21]Q. Q. Wang, Z. Wang, X. Q. Liu, and X. M. Chen, J. Am. Ceram. Soc. **95**, 670 (2012).
[22]Z. Z. Ma, Z. M. Tian, J. Q. Li, C. H. Wang, S. X. Huo, H. N. Duan, and S. L. Yuan, Solid State Sci. **13**, 2196 (2011).
[23]Y. Ma and X. M. Chen, J. Appl. Phys. **105**, 054107 (2009).
[24]H. Matsuo, Y. Noguchi, M. Miyayama, M. Suzuki, and A. Watanabe, J. Appl. Phys. **108**, 104103 (2010).
[25]T. H. Wang, C. S. Tu, H. Y. Chen, Y. Ding, and T. C. Lin, J. Appl. Phys. **109**, 044101 (2011).
[26]A. Singh, V. Pandey, R. K. Kotnala, and D. Pandey, Phys. Rev. Lett. **101**, 247602 (2008).
[27]N. Itoh, T. Shimura, W. Sakamoto, and T. Yogo, Ferroelectrics **356**, 19 (2007).
[28]M. T. Buscaglia, L. Mitoseriu, V. Buscaglia, I. Pallecchi, M. Viciani, P. Nanni, and A. S. Siri, J. Euro. Ceram. Soc. **26**, 3027 (2006).
[29]S. Chandarak, J. Jutimoosik, A. Bootchanont, M. Unruan, P. Jantaratana, S. Priya, S. Srilomsak, S. Rujirawat, and P. Yimnirun, J. Supercond. Nov. Magn. **26**, 455 (2013).
[30]S. O. Leontsev and R. E. Eitel, J. Am. Ceram. Soc. **92**, 2957 (2009).
[31]H. B. Yang, C. R. Zhou, X. Y. Liu, Q. Zhou, G. H. Chen, W. Z. Li, and H. Wang, J. Eur. Ceram. Soc. **33**, 1177 (2013).
[32]S. K. Nalwa and A. Garg, J. Appl. Phys. **103**, 044101 (2008).
[33]G. L. Yuan, Or SW, J. M. Liu, and Z. G. Liu, Appl. Phys. Lett. **89**,052905 (2006).
[34]S. T. Zhang, L. H. Pang, Y. Zhang, M. H. Liu, and Y. F. Chen, J. Appl. Phys. **100**, 114108 (2006).
[35]C. Lan, Y. Jiang, and S. Yang, J. Mater. Sci. **46**, 734 (2011).
[36]M. I. Mendelson, J. Am. Ceram. Soc. **52**, 443–446 (1969).
[37]X. H. Wang, P. L. Chen, and I. W. Chen, J. Am. Ceram. Soc. **89**, 431 (2006).
[38]L. Lutterotti, MAUD, Material Analysis Using Diffraction, 2011. http://www.ing.unitn.it/~maud/index.html.
[39]M. S. Kim, J. G. Fisher, S. J. L. Kang, and H. Y. Lee, J. Am. Ceram. Soc. **89**, 1237 (2006).
[40]M. S. Kim, D. S. Lee, E. C. Park, S. J. Jeong, and J. S. Song, J. Eur. Ceram. Soc. **27**, 4121 (2007).
[41]B. K. Lee, S. Y. Chung, and S. J. L. Kang, Acta. Mater. **48**, 1575 (2000).
[42]B. Jaffe, W. R. Cook, and H. Jaffe, *Piezoelectric Ceramics* (Academic Press, New York, 1971).
[43]C. C. Huang and D. P. Cann, J. Appl. Phys. **104**, 024117 (2008).
[44]J. H. Hao, W. Bai, W. Li, and J. Zhai, J. Am. Ceram. Soc. **95**, 1998 (2012).
[45]C. A. Randall, N. Kim, J. P. Kucera, W. Cao, and T. R. Shrout, J. Am. Ceram. Soc. **81**, 677–688 (1998).
[46]W. Cao and C. A. Randall, J. Phys. Chem. Solids **57**, 1499 (1996).
[47]M. Demartin and D. Damjanovic, Appl. Phys. Lett. **68**, 3046 (1996).
[48]Q. Zhou, C. Zhou, H. Yang, G. Chen, W. Li, and H. Wang, J. Am. Ceram. Soc. **95**, 3889 (2012).
[49]X. Chen, Y. Wang, Y. Yang, G. Yuan, J. Yin, and Z. Liu, Solid State Commun. **152**, 497 (2012).
[50]E. Buixaderas, V. Bovtun, M. Kempa, M. Savinov, D. Nuzhnyy, F. Kadlec, P. Vaněk, J. Petzelt, M. Eriksson, and Z. Shen, J. Appl. Phys. **107**, 014111 (2010).
[51]Y. Park, W. J. Lee, and H. G. Kim, J. Phys. Condensed Mater. **9**, 9445 (1997).
[52]S. Chattopadhyay, P. Ayyub, V. R. Palkar, and M. Multani, Phys. Rev. B **52**, 13177 (1995).
[53]J. Wu, D. Xiao, B. Wu, W. Wu, J. Zhu, Z. Yang, and J. Wang, Mater. Res. Bull. **47**, 1281 (2012).
[54]X. G. Tang and H. L. W. Chan, J. Appl. Phys. **97**, 034109 (2005).
[55]D. Lebeugle, D. Colson, A. Forget, M. Viret, A. M. Bataille, and A. Gukasov, Phys. Rev. Lett. **100**, 227602 (2008).